Received: 22 July 2022 | Revised: 18 April 2023 | Accepted: 19 April 2023

DOI: 10.1002/nbm.4958

RESEARCH ARTICLE

NMR IN BIOMEDICINE WILEY

Feasibility of clinical studies of chemical exchange saturation transfer magnetic resonance imaging of prostate cancer at 7 T

Daan J. Reesink[1] | Catalina S. Arteaga de Castro[2] | Tijl Van der Velden[2] | Jeanette Van Vooren[3] | Petri Oost[4] | Trudy G.N. Jonges[5] | Marnix G. E. H. Lam[3] | Bart de Keizer[3] | Peter-Paul M. Willemse[1] | Richard P. Meijer[1] | Dennis W. J. Klomp[2]

[1]Department of Oncological Urology, Division Imaging and Oncology, University Medical Center Utrecht, Utrecht, The Netherlands

[2]Department of Precision Imaging, Division Imaging and Oncology, University Medical Center Utrecht, Utrecht, The Netherlands

[3]Department of Radiology, Division Imaging and Oncology, University Medical Center Utrecht, Utrecht, The Netherlands

[4]Department of Urology, Tergooi Hospital Hilversum, Hilversum, The Netherlands

[5]Department of Pathology, University Medical Center Utrecht, Utrecht, The Netherlands

Correspondence
Daan J. Reesink, Department of Urology, University Medical Center Utrecht, Heidelberglaan 100, 3584 CX Utrecht, The Netherlands.
Email: d.reesink@antoniusziekenhuis.nl

Funding information
KWF Kankerbestrijding, Grant/Award Number: (Grant number 10810)

Abstract

Chemical exchange saturation transfer (CEST) has been explored for differentiation between tumour and benign tissue in prostate cancer (PCa) patients. With ultrahigh field strengths such as 7-T, the increase of spectral resolution and sensitivity could allow for selective detection of amide proton transfer (APT) at 3.5 ppm and a group of compounds that resonate at 2 ppm (i.e., [poly]amines and/or creatine). The potential of 7-T multipool CEST analysis of the prostate and the detection of PCa was studied in patients with proven localised PCa who were scheduled to undergo robot-assisted radical prostatectomy (RARP). Twelve patients were prospectively included (mean age 68.0 years, mean serum prostate-specific antigen 7.8ng/mL). A total of 24 lesions larger than 2 mm were analysed. Used were 7-T T2-weighted (T2W) imaging and 48 spectral CEST points. Patients received 1.5-T/3-T prostate magnetic resonance imaging and galium-68-prostate-specific membrane antigen-positron emission tomography/computerised tomography to determine the location of the single-slice CEST. Based on the histopathological results after RARP, three regions of interest were drawn on the T2W images from a known malignant zone and benign zone in the central and peripheral zones. These areas were transposed to the CEST data, from which the APT and 2-ppm CEST were calculated. The statistical significance of the CEST between the central zone, the peripheral zone, and tumour was calculated using a Kruskal–Wallis test. The z-spectra showed that APT and even a distinct pool that resonated at 2 ppm were detectable. This study showed a difference trend in the APT levels, but no difference in the 2-ppm levels when tested between the central zone, the peripheral zone, and tumour ($H(2) = 4.8$, $p = 0.093$ and $H(2) = 0.86$, $p = 0.651$, respectively). Thus, to conclude, we could most likely detect APT and amines and/or creatine levels noninvasively in prostate using the CEST effect. At

R. P. Meijer and D. W. J. Klomp shared senior authorship.

group level, CEST showed a higher level of APT in the peripheral versus the central zone; however, no differences of APT and 2-ppm levels were observed in tumours.

KEYWORDS
7 T, diagnostic accuracy, high field, MRI, prostate cancer

1 | INTRODUCTION

Prostate cancer (PCa) is the second most commonly diagnosed cancer in men, with an estimated 1.3 million new cases worldwide in 2018 (13.5% of all cancers diagnosed in men). PCa is the sixth leading cause of death from cancer in men worldwide, with approximately 360,000 deaths yearly.[1]

In general, current diagnostic tools for PCa are digital rectal examination and serum prostate-specific antigen (PSA).[2] If patients are suspected of PCa, transrectal ultrasound (TRUS)-guided prostate biopsies are performed. However, as TRUS is considered suboptimal to detect PCa, the standard of care changed to random 10–14 core template biopsies.[3]

Magnetic resonance imaging (MRI) is a noninvasive method that can have a high tissue contrast to observe anatomy. Studied in the 1980s, it lacked adequate sensitivity and specificity for routine use in PCa detection.[4] Since then, technical improvements in anatomical contrast imaging (T1-weighted imaging, T2-weighted [T2W] imaging), and the addition of functional diffusion-weighted imaging (DWI), dynamic contrast-enhanced imaging, and metabolic imaging, such as MR spectroscopic imaging (MRSI), and chemical exchange by saturation transfer (CEST), have improved its accuracy.[3,5–9] As a result, prostate multiparametric MRI is now recommended prior to prostate biopsy in biopsy-naïve men.[2]

Current MRI scanners used for prostate MRI have a magnetic field strength of 1.5-T and preferably 3-T. A study comparing 1.5- and 3-T MRI within the same patients showed comparable objective image quality in T2W imaging, but the 3-T scanner was superior in DWI and subjective imaging quality, because of increased signal-to-noise ratio (SNR) and contrast-to-noise ratio.[10] Assessment of lesions resulted in similar 'Prostate Imaging Reporting and Data System standard' (PI-RADS) scores at both field strengths.[11]

Ultrahigh field strengths such as 7-T are also used to study humans, but these are not without challenges.[9,12,13] In particular, the uniformity in flip angle distribution is severely compromised because of the short wavelength of the RF pulses that coincide with 7-T MRI. Fortunately, the use of multiple transmit channels facilitates radiofrequency (RF) interference that can be controlled to provide constructive interference in the prostate.[14,15] Just as importantly, RF power deposition can be distributed via the multiple transmit channels, which can minimise local specific absorption rates (SAR), particularly when using dipole antennas.[16] As a consequence, the higher intrinsic increase of the SNR could lead to a benefit of increased spatial and/or temporal resolution.[10] However, increased SNR on DWI comes at the expense of geometric distortion or can lead to artefacts.[17]

Another advantage at 7-T compared with 3-T is its higher spectral resolution, which can be used to explore metabolic MRI by means of MRSI or CEST. Indeed, MRSI at 7-T has revealed better spectral discrimination between choline, creatine, and citrate, which may benefit the cancer biomarker of (choline + creatine)/citrate.[18] Moreover, substantial improvement in the detection of polyamines[19] in PCa was observed, which (as this metabolite has protons that rapidly exchange with water) may be a good candidate for CEST imaging.

To date, very few studies have performed CEST in PCa.[5,20,21] These studies were all obtained at 3 T, which, because of limited spectral resolution and the low number of z-spectral points, provided insufficient spectral resolution to pick up the signals exchanged from (poly)amines and/or creatine protons.

The current study was performed to prospectively evaluate the feasibility of 7-T multipool CEST of the prostate and the detection of PCa, in patients with proven PCa who were scheduled to undergo robot-assisted radical prostatectomy (RARP). To assess and compare diagnostic accuracy, patients also received galium-68-prostate-specific membrane antigen-positron emission tomography/computerised tomography (^{68}Ga-PSMA-PET/CT) imaging. All imaging modalities were postoperatively validated by whole-mount histopathology after radical prostatectomy.

2 | MATERIALS AND METHODS

2.1 | Patients

Twenty patients with biopsy-proven, localised PCa, who were planned for RARP, were included in this study. Exclusion criteria to undergo the MRI examination were claustrophobia, cardiac pacemaker, metal material anywhere in the body, previous treatment for PCa, a history of radiotherapy to the pelvis, or a history of transurethral resection of the prostate or stenting of the prostate.

Patients were included from the University Medical Center Utrecht (UMCU) and Tergooi Hospital Hilversum/Blaricum. All subjects gave written informed consent prior to inclusion in the study. The study was approved by the UMCU institutional review board (Protocol No. 18/338, CCMO: NL63273.041.18), and it was conducted in accordance with Good Clinical Practice Guidelines and the Declaration of Helsinki.

2.2 | Imaging

Before inclusion, as per standard protocol, all patients received 1.5 - or 3-T prostate MRI. Images were scored according to the Prostate Imaging Reporting and Data System standard (PI-RADS, v. 2).[11] Data from the initial radiologist's (R1) report were collected in a case-report form (CRF), including prostate volume, PI-RADS score, laterality of suspected malignant lesions, apparent diffusion coefficient value, and T-stage (according to the TNM-classification[22]). The location of the lesion was extrapolated using a 27 regions of interest (27-ROI) prostate reporting scheme, according to Dickinson et al.[23] A second radiologist (R2) re-evaluated the 1.5-T/3-T MRI and completed the same CRF.

To minimise the risk of missing tumour tissue in the prostate, and deeming tumour as healthy tissue during analyses, patients underwent ^{68}Ga-PSMA-PET-CT. If there was a suspicion of metastatic disease, incurable by RARP and pelvic lymph node dissection, the patient did not undergo surgery.

2.3 | ^{68}Ga-PSMA-PET-CT acquisition and image reconstruction

Images were obtained from skull to thighs, using a Biopgraph mCT40 scanner (Siemens Healthcare) or a Gemini TF 64 slice scanner (Philips). Patients received an intravenous injection of 1.5 MBq/kg ^{68}Ga-PSMA-11 (ANMI, Telix Pharmaceuticals), and after 60 min, PET images were acquired. Subsequently, low-dose CT was performed directly afterwards. Images were acquired according to the European Association of Nuclear Medicine (EANM) Research Ltd. (EARL) criteria.[24]

Two nuclear medicine physicians (NMP1 and NMP2), each with more than 7 years of experience, separately examined the ^{68}Ga-PSMA-PET/CT images. All the scans were reviewed using syngo.via software (Siemens Healthcare). Every lesion suspected of malignancy was collected in the CRF, using the same 27-ROI reporting scheme. For quantitative analysis, the maximum standardised uptake value (SUV_{max}) for each lesion was measured by drawing an ROI around it on axial images.

2.4 | 7-T MR imaging

Imaging was performed on a whole-body 7-T MR scanner (Philips) with an array of eight transmit-receive fractionated dipole antennas merged with an array of 16 receiver loops,[25] positioned symmetrically around the pelvis.[26] A multitransmit system was used for $B1^+$ shimming, incorporating a conservative average RF power level of 3.1 W per channel to stay within SAR guidelines, independent of applied RF phase shims.[27] To maximise the $B1^+$ and homogeneity in the prostate, phase shimming was performed using the Compass tool (TeslaDC, Zaltbommel, The Netherlands). After second-order B0 shimming of the prostate, a $B1^+$ map[28] and high-resolution T2W images (scan duration 140 s, 18 slices [multislice], 3-mm thickness, 0.3-mm gap, 476 × 399 scan resolution, field of view [FOV] 250 × 59.1 × 381.4, water-fat shift 5.26 pixels, TE = 140 ms)[25] were acquired prior to the CEST.

To obtain sufficient datapoints in the z-spectrum of the CEST acquisition, the CEST pulse was composed of a train of 80 × 25-ms single lobe sinc-Gauss pulses with a 10-ms delay between the pulses, operated at an RMS $B1^+$ of 1.62 uT over the 2.8-s prepulse. The somewhat low $B1^+$ was selected to reduce direct saturation effects of nearby resonances close to water, albeit its consequence to the potential Z-spectrum was not simulated. The readout was a single shot 2D turbo field echo with TE/TR/flip angle = 2.56 ms/15 ms/8 degrees, 300 × 4 × 393 mm FOV, 4 × 4 × 4 mm voxel size, using centre out k-space ordering and including startup excitations that took 1.5 s followed by a 3-s T1 recovery delay. With 48 different offset pulses, the total CEST scanning took 344 s. The frequency offsets were as follows (ppm from water):

−33.557	−33.557	−5.033	−4.698	−4.362	−4.027	−3.859	−3.691	−3.523	−3.3557	−3.020	−2.685
−2.349	−2.013	−1.846	−1.678	−1.5108	−1.3428	−1.1748	−1.0068	−0.839	−0.6719	−0.5039	−0.336
0	0.336	0.5036	0.6716	0.839	1.007	1.174	1.342	1.510	1.6779	1.846	2.013
2.349	2.685	3.020	3.356	3.5231	3.691	3.859	4.027	4.3627	4.698	5.033	33.557

The location of the single slice was guided by using outcomes of 1.5- or 3-T MR and ^{68}Ga-PSMA-PET/CT images.

2.5 | Pathological evaluation

Prostatectomy specimens were processed by a standard whole-mount protocol according to International Society of Urological Pathology protocols.[29] The apex, bladder neck, and six to nine slides (depending on the size of the prostate) were sampled. Haematoxylin and eosin stained slides were scanned using a Hamamatsu RS Nanozoomer 2.0. An experienced pathologist evaluated every slide, outlined every lesion, and calculated the size of the lesion. Every lesion was evaluated for capsular contact and extraprostatic extension. Subsequently, a tumour (T)-stage was determined. Afterwards, every lesion was translated to the 27-ROI template.

2.6 | Image assessment

The following conditions were verified before including the CEST data for further analyses: (1) the slice should include at least one tumour based on the pathological evaluation; (2) the B1 maps over the prostate confirm a successful B1 shim; (3) the carrier frequency after B0 shimming was set to water, so the z-spectrum was obtained correctly; and (4) the z-spectrum itself does not show sudden jumps in data that could be caused by motion during the scan.

The outlined lesions on histopathological examination were translated to the CEST images, including outlines for the central/transition and peripheral zone as follows: (1) the orientation of the pathology slices was matched to the clinical MRI and PET data, using the identified lesions to fine tune the registration; (2) the high-resolution T2W imaging slice of 7-T was matched to the best matching clinical MRI slice; (3) the tumour areas as identified on the corresponding pathology slice, as well as areas excluding the tumour on the central zone as well as on the peripheral zone, were drawn onto the high-resolution T2WI slice of the 7-T; and (4) because the resolution and orientation of the CEST and the T2W imaging scans are known, the three ROIs were copied from the T2W images to the CEST data.

The CEST images were analysed using self-designed MATLAB (R2014b; MathWorks, Inc.) scripts that included Lorentzian fitting of water, amides, amines, magnetisation transfer (MT), and nuclear Overhauser effects (NOEs).[30] We used the search range of 3.3 to 3.7 ppm for amide, 1.7 to 2.2 ppm for the 2-ppm pool (i.e., amines and/or creatine), −4.0 to 2.0 ppm for MT, and −4 to −3.2 for NOEs. For frequency alignment, we used the water saturation shift referencing—WASSR—method[31] embedded in the fully sampled Z-spectra and no motion correction was applied.

2.7 | Statistical analyses

Statistical analyses were performed using SPSS (v. 24.0 for Windows, IBM). To characterise the clinical imaging performance of the included patients, the sensitivity, specificity, positive-predictive value, and negative-predictive value were calculated for 3-T MRI (R1 and R2) and ^{68}Ga-PSMA-PET/CT (NMP1 and NMP2) for each tumour lesion, using the whole-mount histopathological specimen as the gold standard. Receiving operating characteristic (ROC) curves for 1.5-T/3-T MRI and ^{68}Ga-PSMA-PET/CT for the detection of PCa were plotted and the AUC was estimated using a nonparametric method. The amide proton transfer (APT) and 2-ppm levels were tested using the Mann–Whitney U-test (central vs. peripheral zone) and Kruskal–Wallis test (central zone vs. peripheral zone vs. tumour).

All reported p values were two-sided and a p value of less than 0.05 was considered statistically significant.

3 | RESULTS

Of the 20 patients, one patient had distant metastases (multiple bone and possible lung) found on ^{68}Ga-PSMA-PET/CT, and did not undergo RARP. Seven patients had technical issues during 7-T MRI: in one case the selected slice was not through the tumour, in one case substantial motion was observed during the CEST scan, in two cases the B1+ shim failed to reach sufficient uniformity or B1+ strength, and in three cases the carrier frequency was more than 100 Hz off from water. In total, 12 patients had high-quality CEST data for analysis. No adverse events occurred. Patient characteristics can be found in Table 1.

3.1 | Visibility of PCa using anatomical imaging

Only lesions larger than 2 mm in diameter were included for analyses. In total, 24 lesions were discovered on whole-mount histopathology (Table 2).

The diagnostic accuracy of visible lesions on 1.5-T/3-T MRI and ^{68}Ga-PSMA-PET/CT can be found in Table 3. An ROC curve, for 1.5-T/3-T MRI and ^{68}Ga-PSMA-PET/CT, is provided in Figure 1 stratified for each radiologist (R1/R2) or nuclear medicine physician (NMP1/NMP2).

TABLE 1 Patient demographics and characteristics.

Total patients, no. (%)	12	(100.0)
Age, mean years (SD)	68.0	(4.0)
Serum-PSA, mean ug/mL (SD)	7.8	(2.8)
Abnormal DRE, no. (%)	3	(25.0)
Biopsy results		
Laterality PCa, no. (%)		
Left-sided	0	(0.0)
Right-sided	4	(33.3)
Bilateral	8	(66.7)
Gleason score, no. (%)		
$3 + 3 = 6$	2	(16.7)
$3 + 4 = 7$	5	(41.7)
$4 + 3 = 7$	4	(33.3)
$4 + 4 = 8$	1	(8.3)
Initial imaging results		
Prostate volume on 1.5-T/3-T MRI, mean mL (SD)	47.6	(30.4)
rT-stage according to 3-T MRI, no. (%)		
rT1c	1	(8.3)
rT2a-b	5	(41.7)
rT2c	3	(25.0)
rT3a	3	(25.0)
Pathology after RARP results		
Focality of tumour, no. (%)		
Unifocal	2	(16.7)
Oligofocal (≤ 4 lesions)	1	(8.3)
Multifocal (> 4 lesions)	9	(75.0)
pT-stage, no. (%)		
pT2a-b (unilateral PCa)	3	(25.0)
pT2c (bilateral PCa)	5	(41.7)
pT3a (EPE)	3	(25.0)
pT3b (SVI)	1	(8.3)
Gleason score, no. (%)		
$3 + 3 = 6$	1	(8.3)
$3 + 4 = 7$	6	(50.0)
$4 + 3 = 7$	4	(33.3)
$4 + 4 = 8$	1	(8.3)

Abbreviations: DRE, digital rectal examination; EPE, extraprostatic extension; MRI, magnetic resonance imaging; PCa, prostate cancer; PSA, prostate-specific antigen; RARP, robot-assisted radical prostatectomy; SD, standard deviation; SVI, seminal vesical invasion.

An example of all the clinical imaging modalities for one patient is provided in Figure 2A–E.

3.2 | Visibility of PCa using CEST

Based on 3-T MRI and ^{68}Ga-PSMA-PET/CT, a one-slice CEST was acquired from each patient. Subsequently, based on the histopathological results after RARP, three ROIs were drawn on the T2W images: a malignant zone, a benign central zone, and a benign peripheral zone (see the example for one patient in Figure 3A–E). From these zones, the 3.5-ppm (APT) and 2-ppm (i.e., amines and/or creatine) CEST were calculated.

TABLE 2 Pathology characteristics for each malignant lesion.

Total lesions on pathology after RARP, no. (%)	24	(100.0)
Laterality lesion, no. (%)		
Left	10	(41.7)
Right	11	(45.8)
Bilateral (crossing the midline)	3	(12.5)
Location lesion, no. (%)		
Peripheral zone	15	(62.5)
Central/transition zone	6	(25.0)
Peripheral + central/transition zone	3	(12.5)
Gleason score, no. (%)		
3 + 3 = 6	1	(4.2)
3 + 4 = 7	14	(58.3)
4 + 3 = 7	6	(25.0)
4 + 4 = 8	3	(12.5)
Capsular contact, no. (%)	11	(45.8)
Extraprostatic extension (pT3), no. (%)	4	(16.7)

Abbreviation: RARP, robot-assisted radical prostatectomy.

TABLE 3 Diagnostic accuracy of lesions on 3-T MRI and ^{68}Ga-PSMA-PET/CT to detect prostate cancer.

	3-T MRI				^{68}Ga-PSMA-PET/CT			
	R 1		R 2		NMP 1		NMP 2	
Sensitivity (95% CI)	50%	(30–70)	54%	(33–74)	50%	(30–70)	63%	(41–80)
Specificity (95% CI)	75%	(47–92)	56%	(31–79)	100%	(76–100)	88%	(60–98)
PPV (95% CI)	75%	(47–92)	65%	(41–84)	100%	(70–100)	88%	(62–98)
NPV (95% CI)	50%	(30–70)	45%	(24–68)	57%	(37–75)	61%	(39–79)

Abbreviations: 95% CI, 95% confidence interval; ^{68}Ga, ^{68}Galium; CT, computerised tomography; MRI, magnetic resonance imaging; NMP, nuclear medicine physician; NPV, negative-predictive value; PET, positron emission tomography; PPV, positive-predictive value; PSMA, prostate-specific membrane antigen; R, radiologist.

Based on data of all 12 patients preselected for good CEST data quality (i.e., providing relatively uniform $B1^+$ and B0 maps over the prostate, as indicated in Figure 4A,B), the z-spectra for all patients could be used to calculate APT and 2-ppm pool levels, which are shown in Figure 5A–C (for each patient shown in Figure S1). The z-spectra show that APT and even 2-ppm levels are detectable.

Subsequently, boxplots for APT-CEST and amine-CEST, in the central zone, peripheral zone, and malignant zone, were drawn by referencing the average ROI values for each individual patient to the average values of their central and peripheral zone ROIs (Figure 5D,E).

The APT levels significantly differed between the central and the peripheral zone ($p = 0.027$). The 2-ppm levels did not differ ($p = 0.844$). This study did not demonstrate any difference in the APT and 2-ppm levels when tested between the central zone, peripheral zone, and tumour ($H(2) = 4.8$, $p = 0.093$ and $H(2) = 0.86$, $p = 0.651$, respectively), because of large standard deviations in the APT and 2-ppm levels from tumour areas, which therefore completely overlap with the levels of healthy prostate tissue.

4 | DISCUSSION

For the first time ever, we can detect a pool of most likely amines and/or creatine levels noninvasively in PCa patients using the CEST effect. In contrast to the results reported at 3-T,[20] where the resonance of amine is overshadowed by the broad direct saturation of water, at 7-T the resonance is just outside the direct saturation zone of water. To maximise the ability to pick up this resonance, we used a relatively high density of frequency samples in the z-spectrum. This facilitated pixel-based frequency alignments in the presence of subtle magnetic field nonuniformities without missing the 2-ppm resonance, while correcting for NOE and saturation transfer effects.[31]

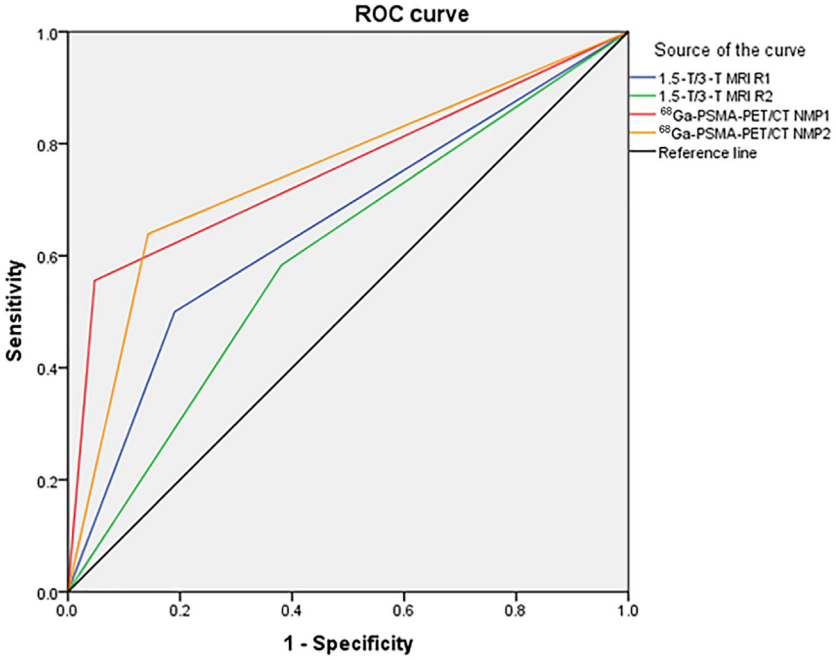

FIGURE 1 Receiver operating characteristic (ROC) curve of 3-T MRI (radiologist 1 [R1] [AUC 0.63 {95% CI 0.45–0.80}, $p = 0.185$] and radiologist 2 [R2] [AUC 0.55 {95% CI 0.37–0.74}, $p = 0.581$]), ^{68}Ga-PSMA-PET/CT (nuclear medicine physician [NMP] 1 [AUC 0.75 {95% CI 0.60–0.90}, $p = 0.008$] and NMP 2 [AUC 0.75 {95% CI 0.60–0.90}, $p = 0.008$]) to identify prostate cancer (PCa). ^{68}Ga-PSMA-PET/CT, galium-68-prostate-specific membrane antigen-positron emission tomography/computerised tomography; AUC, area under the curve; MRI, magnetic resonance imaging.

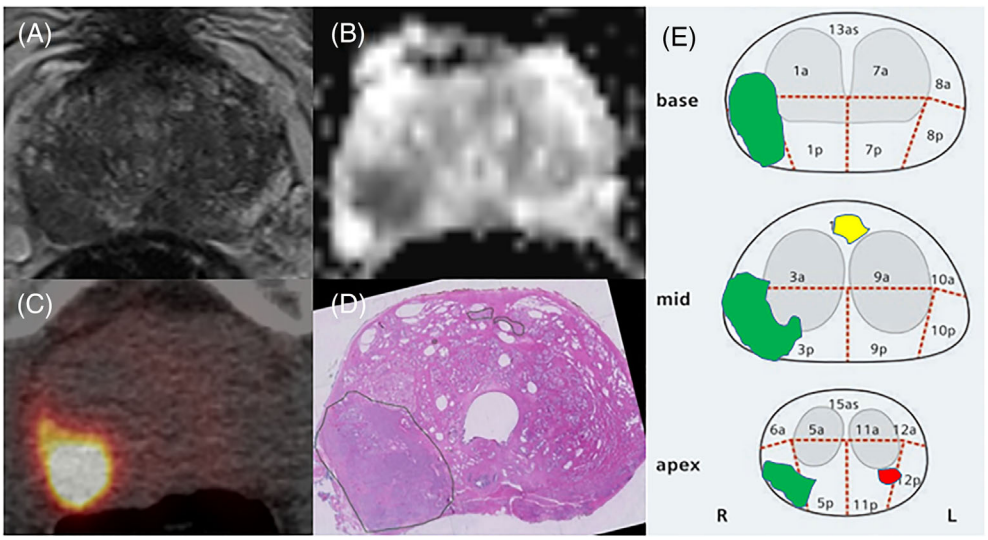

FIGURE 2 Axial slices of the mid-prostate from (A) T2W imaging 3-T MRI, (B) ADC 3-T MRI, (C) ^{68}Ga-PSMA-PET/CT, and (D) histopathological examination of a 67-year-old patient. Serum-PSA was 5.2 ng/mL, the digital rectal examination was benign, and the prostate volume was 37 cc (3-T MRI). A large lesion is visible in the peripheral zone on the right. On 3-T MRI, the lesion was classified as PI-RADS 5, with capsular contact and suspicion of extraprostatic extension. On ^{68}Ga-PSMA-PET/CT, the SUV_{max} was 14.3. On histopathological examination after prostate biopsy, the patient had a unilateral right-sided Gleason score of $4 + 3 = 7$ prostate cancer (PCa) in 1/6 biopsies. However, on histopathological examination after robot-assisted radical prostatectomy (RARP), the patient had a bilateral Gleason score of $4 + 3 = 7$. There was an extraprostatic extension, and the surgical margins were positive (R1). In total, the patient had three malignant lesions on histopathological examination after RARP (E) (green, yellow, red), of which the last two were missed on all imaging modalities. ^{68}Ga-PSMA-PET/CT, galium-68-prostate-specific membrane antigen-positron emission tomography/computerised tomography; ADC, apparent diffusion coefficient; MRI, magnetic resonance imaging; PI-RADS, Prostate Imaging Reporting and Data System standard; PSA, prostate-specific antigen; SUV_{max}, maximum standardised uptake value; T2W, T2-weighted.

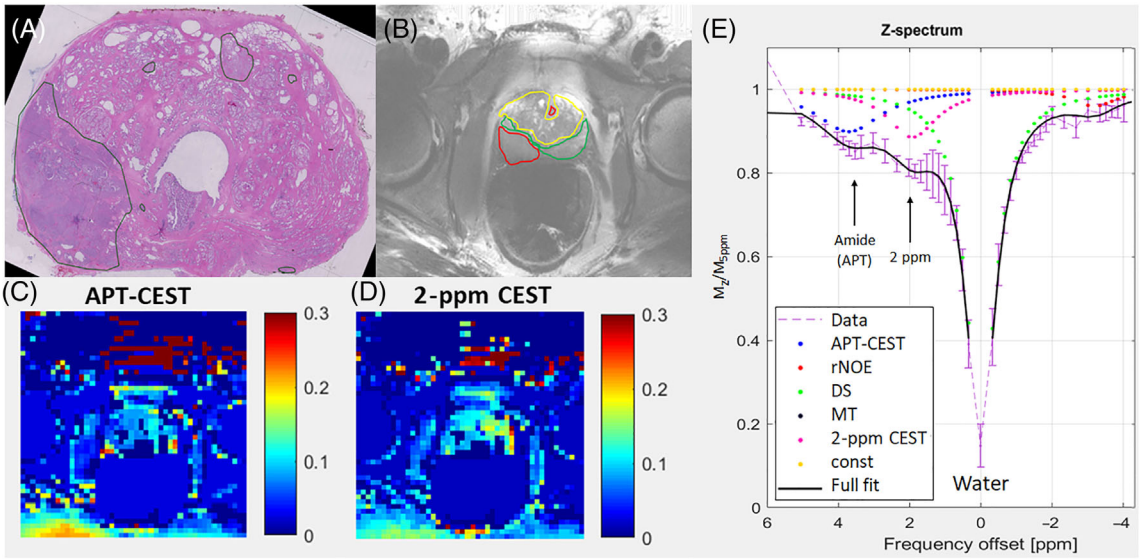

FIGURE 3 Histopathological axial slice (A) of the mid-prostate, transposed to the T2W images to highlight a malignant zone (red) and benign zones in the central (yellow) and peripheral (green) zones. These regions of interest were copied to the (C) APT and (D) 2-ppm CEST images. The averaged Z-spectrum including standard deviation in the central zone (E) shows clear resonances of amide and amines that could be fitted to Lorentzian lines. APT, amide proton transfer; CEST, chemical exchange saturation transfer; DS, direct water-saturation; MT, magnetisation transfer; rNOE, relayed nuclear Overhauser effect; T2W, T2-weighted.

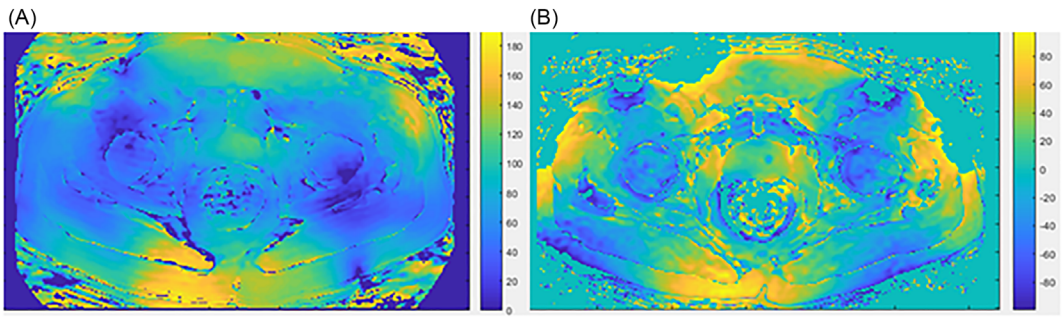

FIGURE 4 (A) Transversal $B1^+$ map (expressed in percentages of the nominal flip angle) and (B) B0 map (expressed as the offset frequency of the water resonance) obtained from a patient showing relatively uniform fields in the region of the prostate.

Alternative strategies could be used to detect amine and/or creatine levels in the prostate. For instance, MRSI at 7-T reveals a resonance at 3.0 ppm from creatine and a complex resonance at 3.1 ppm that originates from nonwater exchangeable proton of polyamines. However, to eliminate artefacts from the orders of magnitude larger water and lipid signals surrounding the prostate, complex scans are required and, to date, always the presence of an endorectal RF coil.[32] At 3-T MRSI these amine signals are also visible, but substantially overlap with choline and creatine resonances at 3.2 and 3.0 ppm, respectively. Consequently, the added value of amines in the detection or grading of PCa has not yet been assessed.

The advantage of CEST over MRSI is that the SNR of CEST is much higher. Moreover, the level of detection in the pool that resonates at 2 ppm is in the range of 10% of the water signal (see Figure 4), while in MRSI this would be four orders of magnitude less (several mM vs. more than 40 M), hence is less prone to artefacts. Moreover, in addition to the pool at 2 ppm, APT levels can be assessed in the same CEST scan, and have shown promising benefits in detecting or grading tumours, particularly in brain.[33]

In the current study, we could indeed pick up these APT levels with a relatively small standard deviation in healthy prostate tissue compared with the standard deviations reported at 3-T,[5,20,21] which, next to the higher spectral dispersion at 7-T, may also be attributed to the higher SNR that can be obtained with our setup compared with 3-T.[25] In fact, in the group average, even an approximately 10% higher level of APT is observed in healthy peripheral zone versus healthy glandular tissue, while we could not see a difference in 2-ppm levels. However, in our study we noticed a large standard deviation in the APT and 2-ppm levels from tumour areas that therefore completely overlaps with the levels of healthy prostate tissue. A large standard deviation was also observed at 3-T, where APT levels were assessed using z-spectrum asymmetry

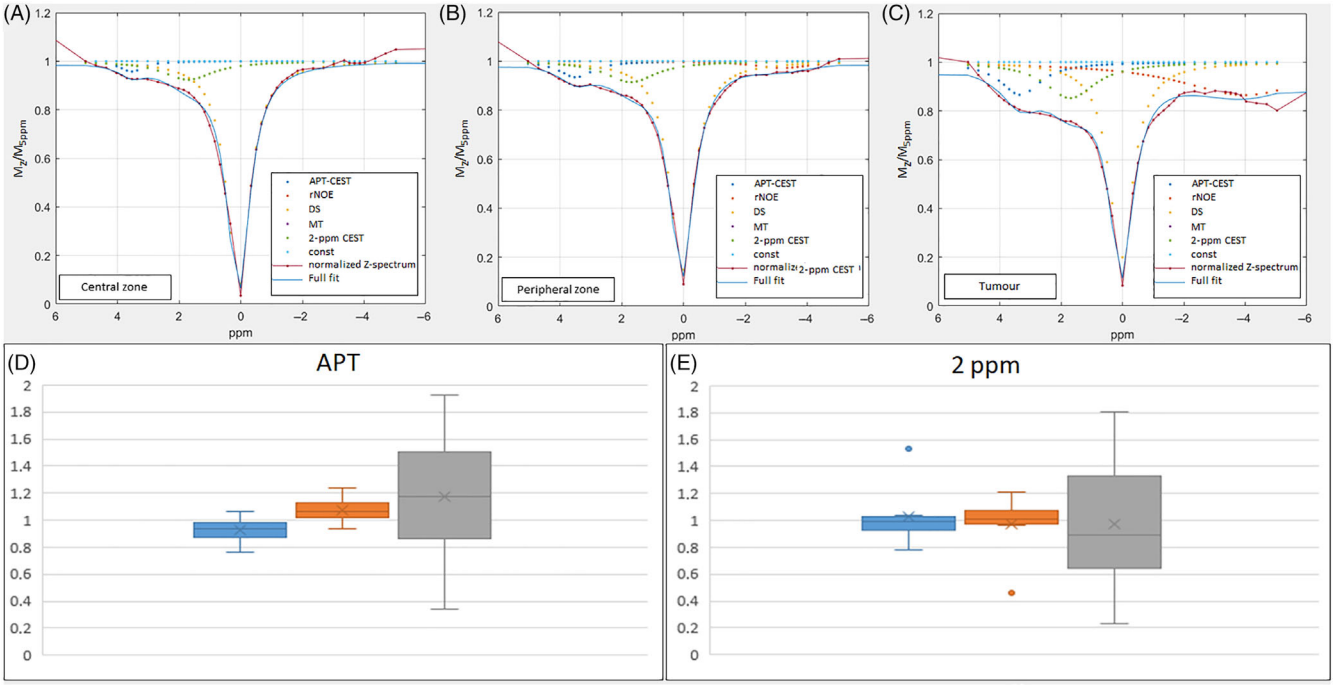

FIGURE 5 7-T CEST Z-spectra for (A) the central zone, (B) the peripheral zone, and (C) tumour, grouped over all patients and boxplots for (D) APT and (E) 2-ppm CEST for the (blue) central zone, (orange) peripheral zone, and (grey) tumour. APT, amide proton transfer; CEST, chemical exchange saturation transfer; DS, direct water-saturation; MT, magnetisation transfer; rNOE, relayed nuclear Overhauser effect.

assessments; and, because of their larger sample size, this could partly be explained by observing higher levels of APT with increasing Gleason scores. However, as clearly indicated by Evans et al.,[20] care must be taken in the interpretation of APT levels when assessed as an asymmetry measurement in the z-spectrum, because these numbers can be highly dependent on MT effects.

Because 1.5-T/3-T MRI and ^{68}Ga-PSMA-PET/CT data were available, we could assess the diagnostic accuracy of CEST MRI. However, as our CEST data did not demonstrate a significant distinction between tumour and healthy tissue, the added value of CEST was not included in the ROC curve. Nonetheless, we did include the data in the current study so to identify the conditions of our included patients.

To ensure perfect CEST data for analyses, we had to exclude a large number of patients from the study. In subsequent studies, the level of exclusion could be reduced as follows: first, the patients in this trial did not receive any bowel-preparation techniques prior to prostate MRI, such as the use of hyoscine N-butylbromide, microenema, or dietary restrictions, as proposed by Schmidt et al.[34] Because the CEST scan is prone to motion artefacts, as noticed in one patient, such bowel motion restriction may prevent these artefacts. Second, while our scan protocol was equipped with a B1 map, we only used this to judge scan performance, while an updated transmit power could have ensured the correct B1. Likewise, B1 correction strategies can be considered to still include the data with suboptimal B1 levels.[35] Third, the f0 determination of the MRI system seems to have caused a failure in three patients. An alternative would be to obtain a fast B0 map and locally ensure that the frequency is set correctly. When sufficient datapoints are obtained in the z-spectra, frequency corrections can be applied over a longer range of offsets. Finally, the pixel size of our CEST scan is larger than the inclusion criteria of minimum tumour size. Consequently, partial volume effects from healthy tissue can reduce the observed effect size in the CEST data from tumours, which may be mitigated when CEST scans are obtained with higher spatial resolutions.

While our study used premature technology to obtain the first CEST data from patients with PCa at 7-T, recent innovations in CEST acquisitions are likely to improve the robustness of CEST MRI in future studies. For instance, much higher acceleration factors (i.e., 6-fold per single direction[25]) could be incorporated to facilitate 3D acquisitions. Also, motion navigators and real-time corrections for motion may be embedded, as was proposed for the head.[36] Likewise, improvements in data processing may be envisioned that incorporate image alignments and high spectral resolution CEST data interpretation with polynominal Lorentzian line-shape fitting (PLOF).[37]

5 | CONCLUSION

We prospectively evaluated the potential of 7-T CEST MRI of the prostate and the visibility of PCa. The current study shows that, because of the higher spectral resolution of 7-T, we could most likely detect amide and a pool that resonates at 2-ppm (i.e., amine and/or creatine) levels

noninvasively in the prostate using the CEST effect. At group level, CEST showed a higher level of APT in the peripheral versus the central zone; however, no differences in APT and 2-ppm levels were observed compared with the tumour zone.

ORCID

Daan J. Reesink https://orcid.org/0000-0002-8977-7013
Catalina S. Arteaga de Castro https://orcid.org/0000-0002-1055-2672
Tijl Van der Velden https://orcid.org/0000-0001-6993-8767
Marnix G. E. H. Lam https://orcid.org/0000-0002-4902-9790
Bart de Keizer https://orcid.org/0000-0002-6270-9483
Peter-Paul M. Willemse https://orcid.org/0000-0002-6364-9224
Richard P. Meijer https://orcid.org/0000-0003-2510-7982
Dennis W. J. Klomp https://orcid.org/0000-0002-5884-5386

REFERENCES

1. Bray F, Ferlay J, Soerjomataram I, Siegel RL, Torre LA, Jemal A. Global cancer statistics 2018: GLOBOCAN estimates of incidence and mortality worldwide for 36 cancers in 185 countries. *CA Cancer J Clin*. 2018;68(6):394-424. doi:10.3322/caac.21492
2. EAU Guidelines. Edn. Presented at the EAU Annual Congress, Amsterdam, 2022. http://uroweb.org/guidelines/compilations-of-all-guidelines/
3. Thompson J, Lawrentschuk N, Frydenberg M, Thompson L, Stricker P. The role of magnetic resonance imaging in the diagnosis and management of prostate cancer. *BJU Int*. 2013;112(2):6-20. doi:10.1111/bju.12381
4. Rifkin MD, Zerhouni EA, Gatsonis CA, et al. Comparison of magnetic resonance imaging and ultrasonography in staging early prostate cancer. Results of a multi-institutional cooperative trial. *N Engl J Med*. 1990;323(10):621-626. doi:10.1056/NEJM199009063231001
5. Jia G, Abaza R, Williams JD, et al. Amide proton transfer MR imaging of prostate cancer: a preliminary study. *J Magn Reson Imaging*. 2011;33(3):647-654. doi:10.1002/jmri.22480
6. Scheenen TWJ, Fütterer J, Weiland E, et al. Discriminating cancer from noncancer tissue in the prostate by 3-dimensional proton magnetic resonance spectroscopic imaging: a prospective multicenter validation study. *Invest Radiol*. 2011;46(1):25-33. doi:10.1097/RLI.0b013e3181f54081
7. Yu KK, Scheidler J, Hricak H, et al. Prostate cancer: prediction of extracapsular extension with endorectal MR imaging and three-dimensional proton MR spectroscopic imaging. *Radiology*. 1999;213(2):481-488. doi:10.1148/radiology.213.2.r99nv26481
8. Kumar R, Nayyar R, Kumar V, et al. Potential of magnetic resonance spectroscopic imaging in predicting absence of prostate cancer in men with serum prostate-specific antigen between 4 and 10 ng/mL: a follow-up study. *Urology*. 2008;72(4):859-863. doi:10.1016/j.urology.2008.01.014
9. Arteaga de Castro CS, Hoogduin HJM, Khlebnikov V, Luijten PR, Klomp DWJ, Zaiss M. Selective amide- and NOE-CEST- MRI in prostate at 7T using a multi-transmit system. ISMRM 24th Annual Meeting Exhibition, Singapore, 2016:4–5.
10. Ullrich T, Quentin M, Oelers C, et al. Magnetic resonance imaging of the prostate at 1.5 versus 3.0T: a prospective comparison study of image quality. *Eur J Radiol*. 2017;90:192-197. doi:10.1016/j.ejrad.2017.02.044
11. Kuru TH, Roethke MC, Rieker P, et al. Histology core-specific evaluation of the European Society of Urogenital Radiology (ESUR) standardised scoring system of multiparametric magnetic resonance imaging (mpMRI) of the prostate. *BJU Int*. 2013;112(8):1080-1087. doi:10.1111/bju.12259
12. Arteaga de Castro CS, van den Bergen B, Luijten PR, van der Heide UA, van Vulpen M, Klomp DWJ. Improving SNR and B1 transmit field for an endorectal coil in 7 T MRI and MRS of prostate cancer. *Magn Reson Med*. 2012;68(1):311-318. doi:10.1002/mrm.23200
13. Vos EK, Lagemaat MW, Barentsz JO, et al. Image quality and cancer visibility of T2-weighted magnetic resonance imaging of the prostate at 7 Tesla. *Eur Radiol*. 2014;24(8):1950-1958. doi:10.1007/s00330-014-3234-6
14. van den Bergen B, Klomp DWJ, Raaijmakers AJE, et al. Uniform prostate imaging and spectroscopy at 7 T: comparison between a microstrip array and an endorectal coil. *NMR Biomed*. 2011;24(4):358-365. doi:10.1002/nbm.1599
15. Metzger GJ, Snyder C, Akgun C, Vaughan T, Ugurbil K, Van de Moortele P-F. Local B1+ shimming for prostate imaging with transceiver arrays at 7T based on subject-dependent transmit phase measurements. *Magn Reson Med*. 2008;59(2):396-409. doi:10.1002/mrm.21476
16. Raaijmakers AJE, Ipek O, Klomp DWJ, et al. Design of a radiative surface coil array element at 7 T: the single-side adapted dipole antenna. *Magn Reson Med*. 2011;66(5):1488-1497. doi:10.1002/mrm.22886
17. Mazaheri Y, Vargas HA, Nyman G, Akin O, Hricak H. Image artifacts on prostate diffusion-weighted magnetic resonance imaging: trade-offs at 1.5 Tesla and 3.0 Tesla. *Acad Radiol*. 2013;20(8):1041-1047. doi:10.1016/j.acra.2013.04.005
18. Kobus T, Wright AJ, Weiland E, Heerschap A, Scheenen TWJ. Metabolite ratios in 1H MR spectroscopic imaging of the prostate. *Magn Reson Med*. 2015;73(1):1-12. doi:10.1002/mrm.25122
19. Klomp DWJ, Bitz AK, Heerschap A, Scheenen TWJ. Proton spectroscopic imaging of the human prostate at 7 T. *NMR Biomed*. 2009;22(5):495-501. doi:10.1002/nbm.1360
20. Evans VS, Torrealdea F, Rega M, et al. Optimization and repeatability of multipool chemical exchange saturation transfer MRI of the prostate at 3.0 T. *J Magn Reson Imaging*. 2019;50(4):1238-1250. doi:10.1002/jmri.26690
21. Takayama Y, Nishie A, Sugimoto M, et al. Amide proton transfer (APT) magnetic resonance imaging of prostate cancer: comparison with Gleason scores. *MAGMA*. 2016;29(4):671-679. doi:10.1007/s10334-016-0537-4
22. Buyyounouski MK, Choyke PL, McKenney JK, et al. Prostate cancer—major changes in the American Joint Committee on Cancer eighth edition cancer staging manual. *CA Cancer J Clin*. 2017;67(3):245-253. doi:10.3322/caac.21391
23. Dickinson L, Ahmed HU, Allen C, et al. Magnetic resonance imaging for the detection, localisation, and characterisation of prostate cancer: recommendations from a European consensus meeting. *Eur Urol*. 2011;59(4):477-494. doi:10.1016/j.eururo.2010.12.009
24. Boellaard R, Delgado-Bolton R, Oyen WJG, et al. FDG PET/CT: EANM procedure guidelines for tumour imaging: version 2.0. *Eur J Nucl Med Mol Imaging*. 2015;42(2):328-354. doi:10.1007/s00259-014-2961-x

25. Steensma BR, Luttje M, Voogt IJ, et al. Comparing signal-to-noise ratio for prostate imaging at 7T and 3T. *J Magn Reson Imaging*. 2019;49(5):1446-1455. doi:10.1002/jmri.26527
26. Raaijmakers AJE, Italiaander M, Voogt IJ, et al. The fractionated dipole antenna: a new antenna for body imaging at 7 Tesla. *Magn Reson Med*. 2016;75(3):1366-1374. doi:10.1002/mrm.25596
27. Meliadò EF, van den Berg CAT, Luijten PR, Raaijmakers AJE. Intersubject specific absorption rate variability analysis through construction of 23 realistic body models for prostate imaging at 7T. *Magn Reson Med*. 2019;81(3):2106-2119. doi:10.1002/mrm.27518
28. Yarnykh VL. Actual flip-angle imaging in the pulsed steady state: a method for rapid three-dimensional mapping of the transmitted radiofrequency field. *Magn Reson Med*. 2007;57(1):192-200. doi:10.1002/mrm.21120
29. Egevad L, Delahunt B, Srigley JR, Samaratunga H. International Society of Urological Pathology (ISUP) grading of prostate cancer—an ISUP consensus on contemporary grading. *APMIS*. 2016;124(6):433-435. doi:10.1111/apm.12533
30. Khlebnikov V, van der Kemp WJM, Hoogduin H, Klomp DWJ, Prompers JJ. Analysis of chemical exchange saturation transfer contributions from brain metabolites to the Z-spectra at various field strengths and pH. *Sci Rep*. 2019;9(1):1-11. doi:10.1038/s41598-018-37295-y
31. Kim M, Gillen J, Landman BA, Zhou J, van Zijl PCM. Water saturation shift referencing (WASSR) for chemical exchange saturation transfer (CEST) experiments. *Magn Reson Med*. 2009;61(6):1441-1450. doi:10.1002/mrm.21873
32. Lagemaat MW, Breukels V, Vos EK, et al. 1H MR spectroscopic imaging of the prostate at 7T using spectral-spatial pulses. *Magn Reson Med*. 2016;75(3):933-945. doi:10.1002/mrm.25569
33. Jiang S, Eberhart CG, Lim M, et al. Identifying recurrent malignant glioma after treatment using amide proton transfer-weighted MR imaging: a validation study with image-guided stereotactic biopsy. *Clin Cancer Res*. 2019;25(2):552-561. doi:10.1158/1078-0432.CCR-18-1233
34. Schmidt C, Hötker AM, Muehlematter UJ, Burger IA, Donati OF, Barth BK. Value of bowel preparation techniques for prostate MRI: a preliminary study. *Abdom Radiol*. 2021;46(8):4002-4013. doi:10.1007/s00261-021-03046-3
35. Khlebnikov V, Windschuh J, Siero JCW, et al. On the transmit field inhomogeneity correction of relaxation-compensated amide and NOE CEST effects at 7 T. *NMR Biomed*. 2017;30(5):1-10. doi:10.1002/nbm.3687
36. Andersen M, Laustsen M, Boer V. Accuracy investigations for volumetric head-motion navigators with and without EPI at 7 T. *Magn Reson Med*. 2022;88(3):1198-1211. doi:10.1002/mrm.29296
37. Wang K, Park S, Kamson DO, Li Y, Liu G, Xu J. Guanidinium and amide CEST mapping of human brain by high spectral resolution CEST at 3 T. *Magn Reson Med*. 2022;1–15(1):177-191. doi:10.1002/mrm.29440

SUPPORTING INFORMATION

Additional supporting information can be found online in the Supporting Information section at the end of this article.

How to cite this article: Reesink DJ, Arteaga de Castro CS, Van der Velden T, et al. Feasibility of clinical studies of chemical exchange saturation transfer magnetic resonance imaging of prostate cancer at 7 T. *NMR in Biomedicine*. 2023;36(10):e4958. doi:10.1002/nbm.4958